From outburst to quiescence: spectroscopic evolution of V1838 Aql imbedded in a bow-shock nebula

J. V. Hernández Santisteban[1,2]⋆, J. Echevarría[2,1], S. Zharikov[3], V. Neustroev[4],
G. Tovmassian[3], V. Chavushyan[5], R. Napiwotzki[6], R.Costero[2], R. Michel[3],
L. J. Sánchez[2], A. Ruelas–Mayorga[2], L. Olguín[7], Ma. T. García–Díaz[3],
D. González–Buitrago[3,8], E. de Miguel[9], E. de la Fuente[10], R. de Anda[2],
and V. Suleimanov[11,12,13]

[1] *Anton Pannekoek Institute for Astronomy, University of Amsterdam, Science Park 904, NL–1098 XH Amsterdam, the Netherlands*
[2] *Instituto de Astronomía, Universidad Nacional Autónoma de México, Apartado Postal 70–264,*
Ciudad Universitaria, México D.F., C.P. 04510, Mexico
[3] *Instituto de Astronomía, Universidad Nacional Autónoma de México, Ensenada, Baja California, C.P. 22830, Mexico*
[4] *Astronomy Research Unit, University of Oulu, PO Box 3000, FIN-90014, Finland*
[5] *Instituto Nacional de Astrofísica, Óptica y Electrónica, Apartado Postal 51, CP 72000, Puebla, Mexico*
[6] *Centre for Astrophysics Research, Science and Technology Research Institute, University of Hertfordshire, Hatfield AL10 9AB, UK*
[7] *Departamento de Investigación en Física, Universidad de Sonora, Blvd. Rosales y Colosio, 83190 Hermosillo, Sonora, Mexico*
[8] *Department of Physics and Astronomy, University of California, Irvine, California 92697, USA*
[9] *Departamento de Ciencias Integradas, Universidad de Huelva, E–21071 Huelva, Spain*
[10] *Instituto de Astronomía y Meteorología, Departamento de Física, CUCEI, Guadalajara, Jalisco, 44100, Mexico*
[11] *Institut für Astronomie und Astrophysik, Universität Tübingen, Sand 1, D-72076 Tübingen, Germany*
[12] *Kazan (Volga region) Federal University, Kremlevskaya str. 18, 420008 Kazan, Russia*
[13] *Space Research Institute of the Russian Academy of Sciences, Profsoyuznaya Str. 84/32, Moscow 117997, Russia*

ABSTRACT

We analyse new optical spectroscopic, direct-image and X-ray observations of the recently discovered a high proper motion cataclysmic variable V1838 Aql. The data were obtained during its 2013 superoutburst and its subsequent quiescent state. An extended emission around the source was observed up to 30 days after the peak of the superoutburst, interpreted it as a bow–shock formed by a quasi-continuous outflow from the source in quiescence. The head of the bow–shock is coincident with the high–proper motion vector of the source ($v_\perp = 123 \pm 5$ km s^{-1}) at a distance of $d = 202 \pm 7$ pc. The object was detected as a weak X-ray source (0.015 ± 0.002 counts s^{-1}) in the plateau of the superoutburst, and its flux lowered by two times in quiescence (0.007 ± 0.002 counts s^{-1}). Spectroscopic observations in quiescence we confirmed the orbital period value $P_{\rm orb} = 0.0545 \pm 0.0026$ days, consistent with early-superhump estimates, and the following orbital parameters: $\gamma = -21 \pm 3$ km s^{-1} and $K_1 = 53 \pm 3$ km s^{-1}. The white dwarf is revealed as the system approaches quiescence, which enables us to infer the effective temperature of the primary $T_{eff} = 11,600 \pm 400$K. The donor temperature is estimated $\lesssim 2200$K and suggestive of a system approaching the period minimum. Doppler maps in quiescence show the presence of the hot spot in HeI line at the expected accretion disc-stream shock position and an unusual structure of the accretion disc in Hα.

Key words: cataclysmic variables, dwarf novae, white dwarf, stars: individual: V1838 Aql

1 INTRODUCTION

Cataclysmic Variables (CVs) are close binary systems where a white dwarf (WD) accretes from a low–mass star via

⋆ e–mail: j.v.hernandez@uva.nl

arXiv:1811.02349v2 [astro-ph.SR] 15 Mar 2019

Roche–lobe overflow, often creating an accretion disc (for a review see Warner 1995). The evolution of CVs is driven by the removal of angular momentum from the system, which leads to the depletion of the donor and causes the orbital period (P_{orb}) to shrink. This process continues until the donor reaches the sub-stellar regime (i.e. a brown dwarf donor) (Howell et al. 1997), where its internal structure causes the donor to expand in response to the loss mass, thus leading to an increase in P_{orb}. This fact causes a sharp cut-off in the P_{orb} distribution called the period minimum (Paczynski & Sienkiewicz 1981). In addition, the long time-scales associated at the period minimum leads to the accumulation of most CVs between 1-2 hrs (Gänsicke et al. 2009), with a large fraction of systems evolving towards longer P_{orb}, known as period bouncers. Out of this short P_{orb} population, up to ~70 % (Kolb & Baraffe 1999; Goliasch & Nelson 2015) should be period bouncers and harbour a substellar donor. Theoretically, the stellar to sub-stellar transition roughly coincides with the period minimum. However, there is little observational evidence of its location given the lack of detailed characterisation of systems around the period minimum (e.g. Littlefair et al. 2006; Harrison 2016; Hernández Santisteban et al. 2016; Neustroev et al. 2017; Pala et al. 2018).

Short orbital period systems (often referred as WZ Sge–type objects) are characterised by enhanced brightness, extended outburst duration (~30 days) as well as the onset of superhumps (low-amplitude variability close the orbital period of the system) shortly after maximum brightness. These are often classified as superoutbursts, to distinguish them from those observed in classical dwarf novae. Therefore, the follow-up and detailed characterisation of these systems is paramount to confirm the nature of the donor and test against theoretical expectations (Knigge et al. 2011).

The discovery of a new transient, V1838 Aql (also known as PNV J19150199+0719471), was initially reported by Koichi Itagaki on May 31 2013, as a possible Nova reaching V~10 mag, who reported also that the object was below 15.5 mag on his unfiltered survey image taken on 21.608 UT[1]. Kato (vsnet–alert 15776) pointed out that the high proper motion made it a good candidate for a WZ Sge–type nearby star, close to the galactic plane, ($\ell = 42.145°$, $b = −1.865°$). This classification was confirmed in subsequent vsnet–alerts, where various stages of superhumps were observed as the superoutburst evolved, and a mean superhump period of 0.05803(1) days was reported by Kato (vsnet–alert 15931).

In this paper we present and discuss CCD direct images, X-ray observations and extensive low and high dispersion spectroscopy during outburst and quiescence of V1838 Aql. We show a most striking result: the detection of a nebulosity in emission during the course of the superoutburst. In addition, we present time-resolved spectroscopy and determine orbital parameters from the emission lines, as well as Doppler tomography. The presence of a white dwarf revealed at quiescence allowed us to determine the white dwarf (WD) temperature. Finally, we discuss whether the system is approaching or receding from the minimum orbital period.

2   OBSERVATIONS AND REDUCTION

We will present the multi-wavelength observations of V1838 Aql from its discovery to its quiescent state, spanning over ~ 4 years. In order to simplify the reference to specific dates or epochs throughout the superoutburst, we make use of truncated Julian Days of the form HJD − 2456000.

2.1   Spectroscopy

Observations were obtained with the Echelle spectrograph attached to the 2.1m Telescope of the Observatorio Astronómico Nacional at San Pedro Mártir, on the nights of 2013 June 3 and June 16–19. The Marconi–2, a 2048 × 2048 detector, was used to obtain a spectral resolution of R~19 000, All observations were carried out with the 300 l/mm cross–dispersor, which has a blaze angle at around 5500 Å. The spectral coverage was about 3900–7300 Å. The exposure time for each spectrum was 300 s for June 3 and 900 s for June 16–19. Low dispersion spectroscopy was also obtained on 2013 June 5–7 and 9 with the Boller & Chivens spectrograph (B&Ch), with two different gratings. On the first three nights, a 400 l/mm grating was used, to obtain a high S/N ratio in order to study the spectral energy distribution of the system, with a broad wavelength coverage of about 4130–7575 Å. The exposure time for each spectrum was 300 s. In addition (on June 9) a 1200 l/mm grating was used, to obtain a higher spectral resolution around the interval 5510–6730 Å. In this setup, the exposure time for each spectrum was 300 s.

Further observations were obtained with the B&Ch during the nights of 2013 June 28, 29 and 30, with the 1200 l/mm grating to cover the range around Hα (June 29) and Hβ (June 28 and 30). Additional low resolution observations were obtained also with the B&Ch on 2013 August 15 (4000–7000 Å coverage) with an exposure time of 900 s per spectrum, and two years later on 2015 September 17 (4000–7500 Å coverage) with an exposure time of 1800 s per spectrum, both with the 400 l/mm grating and when the system had already dropped to V~ 17 mag. All observations were made with a 1″5 slit oriented in the EW direction. Arc spectra were taken frequently for wavelength calibration.

The optical spectroscopy of V1838 Aql in quiescence was obtained on 2016 June 27 (HJD=2457566) using the long–slit mode of the OSIRIS instrument attached to the GTC 10.4m telescope. Single spectra were obtained first to cover the optical region $\lambda\lambda = 3400−10000$ Å with the R2500U (600 s), R2500V (500 s), R2500R (500 s), and R2500I (600 s) volume–phased holographic gratings (see bottom spectra in Fig. 3). Phase–resolved spectroscopy was then obtained with the R2005R grating, in the wavelength interval 5575−7685 Å, centred around the Hα emission line. The exposure time for each spectrum was 235 sec, with a total coverage of around one and a half orbital cycles. Standard data reduction procedures for all spectroscopic observations were performed using the IRAF[2] software. The log of all spectroscopic observations is shown in Table 1.

---

[1] www.cbat.eps.harvard.edu/unconf/followups/J19150199+0719471.html
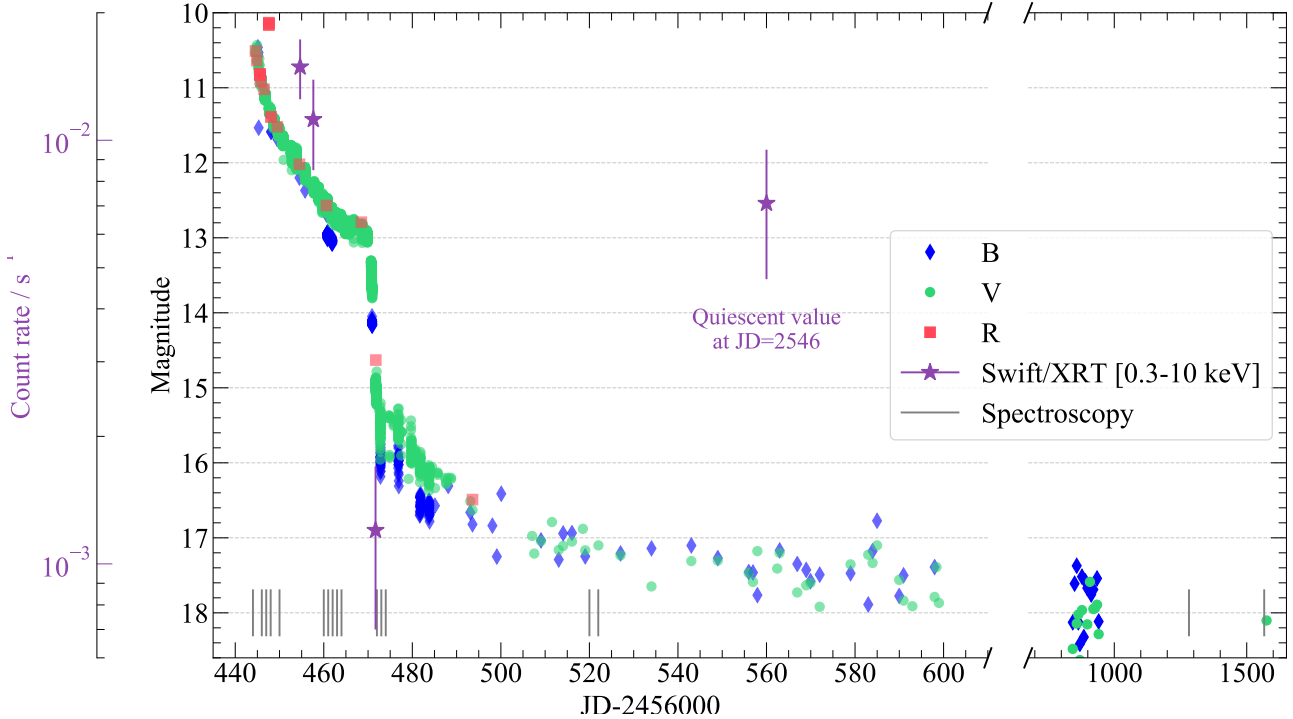
Figure 1. AAVSO and *Swift*/XRT light curves during and after the 2013 superoutburst of V1838 Aql . The observations were taken in V (green dots), R (red squares) and B (blue diamonds) standard filters. The grey vertical marks indicate the epochs of our spectroscopic observations. The 0.3-10 keV *Swift*/XRT count rate is shown in purple stars. Note that the magnitude of the star is still above the minimum derived from the pre-outburst magnitude V=18.6 at the time of the GTC spectral observations on day 1566. The last *Swift*/XRT point is shown as a reference

2.2 Photometry and narrow-band imaging

Direct deep narrow filters images in Hα, Hα Continuum, [OIII] 5007 Å, and [NII] 6583 Å were obtained during 2013, June 3, 18 and 29 at the 0.84m Telescope of the Observatorio Astronómico Nacional at San Pedro Mártir, Mexico. The log of all imaging observations is also presented in Table 1.

We also performed multi-colour optical and near-infrared photometry. On 2016 November 8, we obtained BVRI images with the Andalucia Faint Object Spectrograph and Camera (ALFOSC) at the 2.56 m Nordic Optical Telescope (NOT), in the Observatorio de Roque de los Muchachos (ORM, La Palma, Spain). The integration times were 300 s in each filter. We observed the target again on 2017 October 6 with the New Technology Telescope (NTT) at La Silla Observatory, Chile. The images were captured with the ESO Faint Object Spectrograph and Camera (EFOSC2 – Buzzoni et al. 1984) through the BVRiz filters with exposure times of 40, 40, 40, 60 and 120 sec, respectively. In addition, we obtained two sets of near-infrared (NIR) observations with the JHK$_s$ filters. The observations were performed on 2017 March 8 with the NOTcam instrument on the NOT, and on 2017 Oct 6 with SOFI on the NTT (Moorwood, Cuby & Lidman 1998). The log of all photometric observations is also shown in Table 1.

Pre-outburst observations were derived from the Pan-STARRS1 database[3]. The mean epoch of the observations is

around day 29 in our notation (i.e on 2012, April 12), more than a year earlier to the superoutburst. We extracted the data using a small radius of 0.03 arcmin and obtained the following mean PSF magnitudes in the g, r, i, z, and y filters: 18.56 ± 0.04, 18.67 ± 0.01, 18.76 ± 0.03, 18.61 ± 0.05 and 18.43 ± 0.07, respectively.

2.3 X-rays

V1838 Aql was also observed five times with the Neil Gehrels Swift Observatory (Gehrels et al. 2004). These observations were taken in the middle of the superoutburst plateau stage on 2013 June 11 and 14 (the total exposure time of this data subset is 5.35 ks), at the end of the rapid fading stage

---

[3] The Pan-STARRS1 Surveys (PS1) and the PS1 public science archive have been made possible through contributions by the In-

stitute for Astronomy, the University of Hawaii, the Pan-STARRS Project Office, the Max-Planck Society and its participating institutes, the Max Planck Institute for Astronomy, Heidelberg and the Max Planck Institute for Extraterrestrial Physics, Garching, The Johns Hopkins University, Durham University, the University of Edinburgh, the Queen's University Belfast, the Harvard-Smithsonian Center for Astrophysics, the Las Cumbres Observatory Global Telescope Network Incorporated, the National Central University of Taiwan, the Space Telescope Science Institute, the National Aeronautics and Space Administration under Grant No. NNX08AR22G issued through the Planetary Science Division of the NASA Science Mission Directorate, the National Science Foundation Grant No. AST-1238877, the University of Maryland, Eotvos Lorand University (ELTE), the Los Alamos National Laboratory, and the Gordon and Betty Moore Foundation.

Table 1. Log of photometric and spectroscopic observations

Spectroscopy Date	Julian Date (2456000+)	Range (Å)	No. of Spectra	Exposure Time (s)	Comments
2013 June 3	444	3900–7300	14	300	Echelle
2013 June 5–7	446–448	4130–7575	29	300	Boller & Chivens
2013 June 9	450	5510–6730	29	300	Boller & Chivens
2013 June 16–19	460–464	3900–7300	17	900	Echelle
2013 June 28	472	4500–5700	14	420	Boller & Chivens
2013 June 29	473	5500–6700	14	420	Boller & Chivens
2013 June 30	474	4500–5700	14	420	Boller & Chivens
2013 August 15	520	4000–7000	10	900	Boller & Chivens
2015 September 17	1282	4000–7500	03	1800	Boller & Chivens
2016 June 27	1566	3440–4610	01	600	Osiris – GTC
2016 June 27	1566	4500–6000	02	245	Osiris – GTC
2016 June 27	1566	5575–7685	02	254	Osiris – GTC
2016 June 27	1566	7330–10000	01	600	Osiris – GTC
2016 June 27	1566	5575–7685	30	235	Osiris – GTC

Imaging Date	Julian Date (2456000+)	Filter	FWHM (Å)	Exposure Time (s)	Comments
2013 June 3	444	V	980	30	
2013 June 18	462	Hα	11	1260	180 s × 7 images
2013 June 29	473	Hα	11	1800	180 s × 10 images
2013 June 29	473	Continuum (6650Å)	70	1800	180 s × 10 images
2013 June 29	473	[OIII] 5007	52	1800	180 s × 10 images
2013 June 29	473	[NII] 6583	10	1800	180 s × 10 images

Multicolor Band Photometry		Filters	Telescope	Site	Comments
2016 November 9	1701	BVRI	NOT	ORM	Section
2017 March 8	1820	JHK$_s$	NOT	ORM	2.2
2017 October 6	2032	BVRiz	NTT	La Silla	for more
2017 October 6	2032	JHK$_s$	NTT	La Silla	details

on June 28 (∼5.13 ks), and in quiescence on 2019 March 4 (∼2.85 ks). During the plateau stage, *Swift*-XRT detected a weak X-ray source with a count-rate of 0.0149±0.0024 counts s^{-1}, which is dropped to the level of about 0.0012±0.0006 counts s^{-1} at the end of the rapid fading stage. In quiescence, however, the count-rate has been found at the level of 0.0071±0.0022 counts s^{-1}, that is lower than during the superoutburst plateau but is higher than during the rapid fading stage (see Table 2 for the observation log and Fig. 1). This pattern — the outburst flux is higher than in quiescence with a deep dip during the outburst rapid fading — is in contrast to ordinary dwarf novae which usually show a depression of the X-ray flux during outbursts, but is in agreement with X-ray observations of WZ Sge-type stars (see Neustroev et al. 2018, and references therein).

The plateau-, decline-stage, and quiescent spectra of V1838 Aql consist of only 58, 6, and 12 counts, respectively, therefore no meaningful spectral analysis is possible. Nevertheless, assuming that the spectrum of V1838 Aql is similar to other WZ Sge-type stars such as SSS J122221.7−311525 and GW Lib (Neustroev et al. 2018), and using the count-rate as the scale-factor, one can estimate the X-ray flux of V1838 Aql in the 0.3–10 keV energy range during the superoutburst plateau and in quiescence to be ∼4.5×10^{-13} and ∼2.3×10^{-13} erg s^{-1}cm^{-2}, respectively, with the correspond-

Table 2. Log of *Swift*/XRT observations

Julian Date 2456000+	Exp. Time ks	Obs. ID	X-ray count rate count s^{-1}
454.658	3.370	00032861001/2	$0.0149^{+0.0024}_{-0.0024}$
457.640	1.981	00032861003	$0.0112^{+0.0027}_{-0.0027}$
471.689	5.127	00032870001/15	$0.0012^{+0.0007}_{-0.0005}$
2546.656	2.853	00032870016	$0.0071^{+0.0024}_{-0.0020}$

ing luminosity of ∼2.3×10^{30} and ∼1.2×10^{30} erg s^{-1} (adopting the distance of 202 pc, see Section 3.1). These luminosities are in agreement with those found for other WZ Sge-type stars and accreting white dwarfs (Reis et al. 2013; Neustroev et al. 2018).

3 DISCOVERY OF A NEBULOSITY DURING THE EARLY STAGES OF OUTBURST

We report the detection of an extended component around the object shortly after maximum light. This nebulosity was

first detected in the Echelle spectra on days 460–464, (see day 460 in Fig. 2, lower panel, two days before the first Hα image). Further Hα images were taken on day 462 which revealed a clear diffuse emission centred on the object, as seen in top two panels of Fig. 2. This explains the asymmetry of the line profile observed in the Echelle spectroscopy, due to the slit position (east–west) only covering a fraction of the extended structure at the west of the object. We used DAOPHOT (Stetson 1987) to subtract the point sources, as shown in the middle panel of Fig. 2. Its morphology resembles that of a bow shock e.g. BZ Cam (Hollis et al. 1992). Additional images were taken on day 473 with a narrow filters around the continuum near 6650 Å and also with two narrow filters [OIII] 5007 Å and [NII] 6563 Å. No emission from these forbidden lines was detected. The extended Hα emission was present for nearly a month after the peak of the outburst with no apparent change in morphology. No nebular stage was detected later.

3.1 Proper motion and bow shock

As mentioned in Section 1, V1838 Aql shows a strong proper motion, initially observed from our field images obtained in 2013 and archival data from the Palomar survey (POSS–I and POSS–II). Recently, the *Gaia* DR2 release (Lindegren et al. 2016; Gaia Collaboration et al. 2018) confirmed the high proper motion as well as provided a parallax for the source[4]. The proper motion of V1838 Aql is $\mu_\alpha \cos\delta = -90.1\pm0.2$ mas yr^{-1} and $\mu_\delta = -91.4 \pm 0.2$ mas yr^{-1}. In conjunction with the parallax ($\pi = 4.95\pm0.16$ mas), we performed a joint Bayesian inference for the distance and the tangential velocity following Bailer-Jones et al. (2018)[5] which leads to a tangential velocity of $v_\perp = 123 \pm 5$ km s^{-1} and a distance of 202 ± 7 pc. The joint and marginal posterior distributions are shown in Appendix A. The distance inferred is consistent with our initial SED fitting estimates in quiescence presented in Section 4.4. Thus, combining the systemic radial velocity measurements (see Section 4) with the proper motion, we obtain a space velocity of 125 ± 5 km s^{-1}. V1838 Aql is the third CV with the highest transverse velocity in the Galaxy, just below SDSS 1507+22 ($v_\perp = 182 \pm 30$ km s^{-1}), a confirmed metal–poor halo–binary (Patterson et al. 2008; Uthas et al. 2011), and BF Eri, with an estimated value of $v_\perp \sim 400$ km s^{-1} (Klemola et al. 2004; Neustroev & Zharikov 2008). Follow up Hα observations are needed to perform a more detailed study of its kinematics and origin, and in particular, far– and near–ultraviolet observations are desired to search for anomalous line ratios that might indicate evidence for Population II membership.

The extended emission depicted in the upper and middle panels of Fig. 2 has a (Balmer) bow shock–like shape, formed by our high space velocity object, which we believe is moving supersonically through the interstellar medium (Wilkin 1996). Its shape and duration is very different from the recently discovered nova shells around CVs (Sahman et al. 2015). In fact, the proper motion vector (displayed by the arrow in Fig. 2), coincides with the main axis of the bow
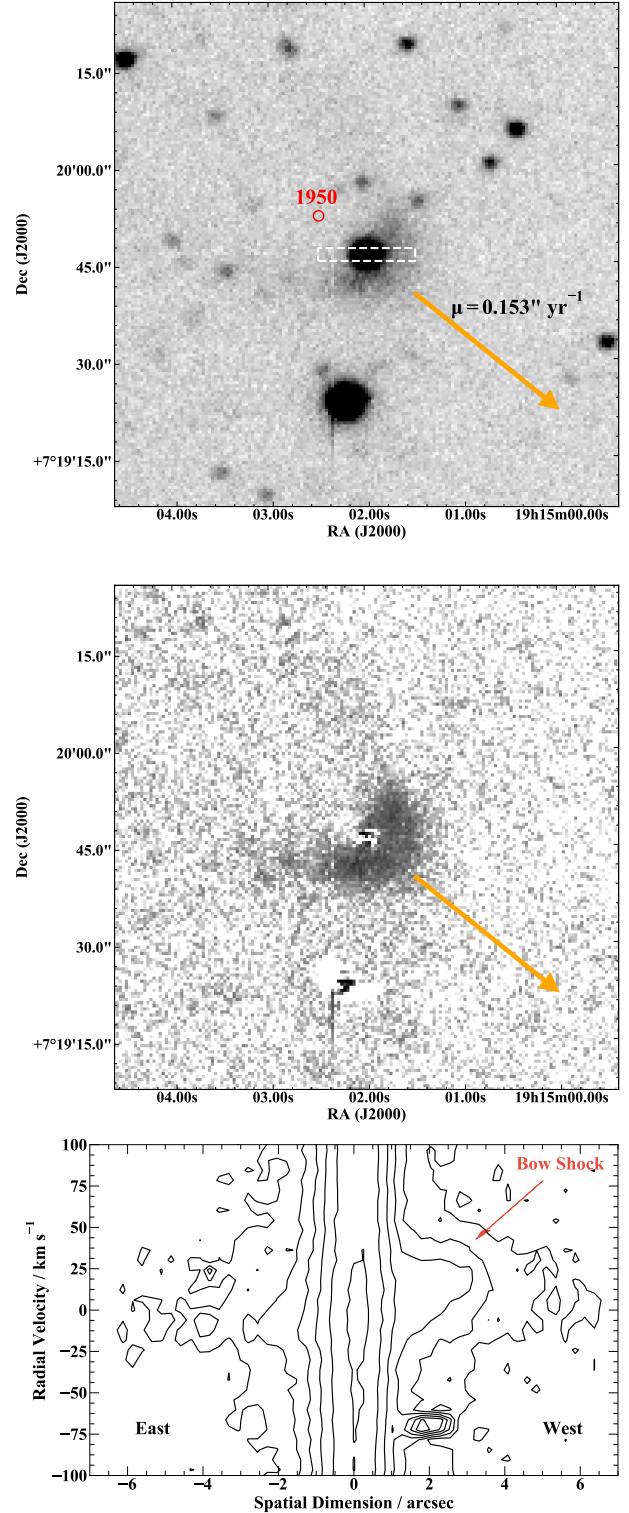
Figure 2. Deep Hα imaging of V1838 Aql. *Top:* The centroid position for the Palomar plates is shown as the circle. The proper motion vector (scaled for clarity) is shown and coincides with the direction of the diffuse emission form the bow shock. The Echelle slit is marked as the dotted box. *Middle:* Stars have been subtracted to show only the extended emission. *Bottom:* 2D Hα profile obtained with the Echelle spectrograph. The wing extending towards the west coincides with the bow shock observed at later times with photometric observations.

---

[4] V1838 Aql catalogue ID is *Gaia* DR2 4306244746253355776
[5] The R-based code is available at https://github.com/ehalley/parallax-tutorial-2018

shock. The head of the nebula is located about $\sim 7''$ from the object and the size of the bow shock cone is $\approx 30''$ along the sky plane with respect to the nebular symmetry axis. The cone open angle is about ~ 60 degrees with its width and brightness quickly decreasing with increasing distance from the bow shock head.

Similar bow shocks are frequently detected around OB–runaway stars (van Buren & McCray 1988) and high–velocity pulsars (Yoon & Heinz 2017, and references therein). However, such bow shocks have also been observed in high–mass transfer CVs (e.g. BZ Cam and V341 Arae Hollis et al. 1992; Greiner et al. 2001; Bond & Miszalski 2018, respectively). It is generally accepted that the interstellar gas, compressed in bow shocks, is heated and ionised by the intense stellar radiation/wind and produces emission as a result of the collisional and/or the charge–exchange excitation of neutral hydrogen atoms in the post–shock flows, with a subsequent emission produced via bound–bound transitions (Chevalier et al. 1980).

The time-scale associated with the presence of the bow shock suggests it was illuminated by the outburst and not material expelled in the outburst itself. Assuming very-fast outflows speeds for the ejecta ($v \sim 0.1c$), the time-scale is of the order of ~ 80 days to reach the observed distance (2×10^{16} cm). This time-scale is larger than the limit imposed by the first detection of the bow shock (< 12 days). Although high velocity outflows can be achieved in energetic novae events (e.g. Metzger et al. 2014), these velocities seem unlikely scenario for an outburst of short orbital period system (which implies low-mass transfer rates Breedt et al. 2014).

Furthermore, the high proper motion of the system (153 mas yr^{-1}) implies that, within an average recurrence time between outbursts ($\sim 30 - 50$ yr for WZ Sge-type CVs), the system would be displaced from the origin of a previous superoutburst by ~ 4.6 arcsec. If this is the case, then the illumination of the apparent nebula would be centred on the location of the previous outburst, contrary to what is observed during the 2013 outburst. Moreover, the morphology of such expanding nebula would differ from a bow shock as shown in other outbursting systems like nova events (Sahman et al. 2015). However, we do not observe any change in the illuminated nebula for over a month.

Therefore, in order to have a standing bow shock, the V1838 Aql must have a quasi-continuous mass outflow. From momentum balance arguments (Weaver et al. 1977; van Buren & McCray 1988), we can estimate a mass outflow rate of $\sim 10^{-11}$ M$_\odot$ yr^{-1} to reproduce the observed bow shock (assuming a ISM density of n= 0.2 cm^{-3}, e.g. Hollis et al. 1992). This value is roughly on the same order of magnitude as the putative mass transfer rate from the donor from evolutionary models (Knigge et al. 2011), which suggests an outflow mechanism capable of expelling a significant percentage of the in-falling material with velocities of $\sim 10^3$ km s^{-1}. Both requirements highly suggest that either a wind or jet-like outflow might be working in the system during the quiescent state.

4 SPECTROSCOPY

We took a series of optical spectra during the evolution of the superoutburst of V1838 Aql from nearly maximum light down to a quiescent level (see Table 1). The spectral evolution of the emission and absorption lines as well as the shape of the continuum is summarised in the next two subsections. We also show in Fig. 3 a comprehensive graph of all the flux calibrated spectra (excluding the Echelle spectra), which illustrate the overall behaviour during this complex event.

4.1 Outburst

The first 14 outburst spectra obtained with the Echelle spectrograph, taken only three days (day 444) after the first report of the eruption (Itagaki 2013), covered an interval of 2.5 hr. These high–resolution spectra show very strong double–peaked Hα emission and a mixed emission and absorption component at the Hβ line. Both emission line components have a FWHM ~ 350 km s^{-1} and are superimposed on a very broad absorption component (± 1000 km s^{-1}). The broad component in Hα is much weaker than in Hβ. No Hγ is present at all. Other features present on the spectra (not shown here) are weak He$_I$ 5876 Å and He$_I$ 4471 Å lines with mixed emission and absorption components. The double–peaked and low–velocity separation (peak to peak) of the Hα line suggests an origin on the outer edges of the disc.

On days 446–448 the B&Ch spectra show a substantial change, as shown in the co–added spectra for the three nights in Fig. 3. The broad absorption components dominate the Balmer series as well as He$_I$ lines, except Hα which show a single peak weak emission. We measured the radial velocity shifts of the centre of this emission line (including night 450) using a single Gaussian with a FWHM~ 6 Å. The first three nights show clear Doppler variations and a drift of the systemic velocity (from $\langle \gamma \rangle \sim +75$ to -10 km s^{-1}). However, our orbital coverage during these nights are very poor and no coherent modulation is observed. On day 450, the radial velocity measurements show a clear modulation with an apparent period coinciding with the early super–hump/orbital period. Due the short time–span of the data, we were not able to find a period value with enough reliability.

The inversion of Balmer emission lines to absorption is common for dwarf novae in outburst (e.g. Clarke & Bowyer 1984; Neustroev et al. 2017). This contrasts to what was observed during the superoutburst of the bounce–back candidate V455 And (Tovmassian et al. 2011). In the latter, the Balmer lines, after an initial switch from emission to broad absorption, they suddenly reversed their course and shoot up back into emission. From the analysis of the width of lines and their radial velocities, Tovmassian et al. (2011) concluded that this is evidence of evaporation and disc wind. This is noteworthy, because the observed bow shock of V1838 Aql supposes some kind of outflow from the object (see discussion in Section 3.1). However, no similar wind or outflow features are seen at the beginning of the superoutburst in this case.

As the outburst progressed, the broad absorption line components shrink and eventually disappear. On the contrary, the Hα line in emission broadens throughout the decline to its quiescent value of FWHM~ 1200 km s^{-1} (see

Section 4.2). This is explicitly shown in the inset of Fig. 3. On days 472–474 additional B&Ch spectra were obtained, Hα and Hβ became again strong with double peak emission.

4.2 Quiescence

The system returned to its quiescence state after 500 days, thus presenting an opportunity to analyse the system in its quiescent state. The full optical spectrum, taken over 1000 days after the outburst, shows a clear presence of accretion disc emission lines superimposed on the WD broad absorption lines, as shown in Fig. 3. Time-resolved spectroscopy however, was focused on the region around the Hα line, where the least contribution of the WD broad absorption lines is observed. Hence, we were able to apply a two Gaussian method (Shafter et al. 1986; Horne et al. 1986) to determine the radial velocity of the primary. We made an interactive search for the optimal width and separation of the Gaussians in a grid between a FHWM of 500–1000 km s^{-1} in 50 km s^{-1} steps and 500–2600 km s^{-1} in 100 km s^{-1} steps, respectively (for further explanation of this method see Hernández Santisteban et al. 2017). At every combination, we performed a fit of the radial velocities, $V(t)$, to a circular orbit:

$$V(t) = K_{em} \sin\left[2\pi(\phi - \phi_0)\right] + \gamma, \qquad (1)$$

where K_{em} is the semi–amplitude, ϕ_0 is the phase offset between the spectroscopy and photometric ephemeris, and γ is the systemic velocity. We used the minimum in the diagnostic quantity σ_{Kem}/K_{em}, where σ_{Kem} is the 1σ uncertainty on the semi–amplitude, to determine the optimal solution (Shafter et al. 1986).

Initially, we have used an arbitrary zero-point close to the observations to calculate the phase offset and have assumed the orbital period of the early superhumps. We obtain an orbital solution with $P_{\rm orb}$ = 0.0545 ± 0.0026 days, K_{em} = 53 ± 3 km s^{-1} and γ = −21 ± 3 km s^{-1} as shown in Fig. 4. This spectroscopic orbital period is consistent with the early superhump period found during the superoutburst (P = 0.05698 ± 0.00009 d, Kato et al. 2014a; Echevarría et al. 2019).

After correcting for the phase offset to fix the zero point of the inferior conjunction of the secondary, we can construct the spectroscopic ephemeris:

$$T(HJD) = 2457566.5290(5) + 0.0545(26)E. \qquad (2)$$

4.3 Doppler tomography

The quiescent spectrum of V1838 Aql contains emission lines that allow us to study the structure of the accretion flow in Hα and He I 5875 Å and 6678 Å, as shown in Fig. 5. We have used Tom Marsh's MOLLY software package[6] to normalise and subtract the continuum of each individual spectrum, as well as re–bin in equal velocity bins. All three lines show a distinct double–peak profile which suggests the presence of

---

[6] http://www2.warwick.ac.uk/fac/sci/physics/research/astro/people/marsh/software/

an accretion disc, shown in the mean profiles in the top panel of Fig. 5. In addition, the lines contain an extra component with a semi–amplitude of ∼ 200 km s^{-1}, which modifies the symmetry of the median profile (most evident in the He lines and are clearly seen in the trail spectra (mid–panels, Fig. 5). However, we note that the extra component in Hα seems to be shifted in orbital phase with respect to both HeI lines.

The time–resolved spectroscopic data allow us to study the structure of the accretion disc via Doppler tomography (Horne & Marsh 1986). We have used the ephemeris obtained via the Hα wings (see Section 4.2) to calculate the tomograms for each individual emission line. We employed the Doppler tomography package TRM-DOPPLER[7] to produce the maps shown in the bottom panels of Fig. 5. The Hα tomogram reveals a clear accretion disc as well as an additional component at $V_x, V_y \approx [0, -500]$ km s^{-1}. Surprisingly, we find a lack of distinct emission of the hot spot in Hα, commonly observed in most CVs. The HeI tomograms produce a sinusoidal contribution superimposed on the weaker accretion disc. The location of the emission in HeI coincides with the expected position in velocity space of the hot spot, where the ballistic trajectory of material ejected from the L1 point intersects the outer edge of the accretion disc.

The fact that the ephemeris is obtained via the wings of the Hα line and simultaneously providing a consistent position for He I hot spots, indicates that the Hα position might be real and not an error of the zero–point used. However, we need more radial velocity observations of V1838 Aql in quiescence to lock down the real zero point.

4.4 White dwarf temperature

In quiescence, the optical spectrum of V1838 Aql is dominated by the broad absorption hydrogen lines arising from the atmosphere of the WD. However, even at these low luminosities, the accretion disc can contribute a significant fraction of the continuum and line emission at optical wavelengths (e.g. Aviles et al. 2010; Hernández Santisteban et al. 2016). Thus, in order to retrieve the physical parameters of the WD, we have modelled the SED in quiescence, F_q, as a combination of a WD atmosphere model F_{wd} broadened to the instrumental resolution ($R \sim 2500$) and a power-law component:

$$F_{\rm q}(\lambda) = \frac{R_{wd}}{d}^2 F_{wd} + A \cdot (\lambda)^\Gamma, \qquad (3)$$

where R_{wd} is the radius of the WD, d the distance, A is the normalisation factor of the power law and Γ is the power law index. We have masked the cores of the Balmer lines and fitted the range between 3900 – 7500 Å. We fixed the distance from the *Gaia* DR2 estimate, $R_{WD} = 0.01$ R$_\odot$ (radius for a 0.8 M$_\odot$ and $\log(g) = 8.35$ WD star) and left Γ and the normalisation as free parameters. We then performed a grid search over a set of WD atmosphere models made with TLUSTY/SYNSPEC (Hubeny & Lanz 1995, 2017). This grid consisted of a single value of surface gravity $\log(g) = 8.35$ which corresponds to the mean WD mass for CVs (Zorotovic et al. 2011) and a range of effective temperatures, T$_{eff}$, 8000–30000 in steps of 100 K. The best fit model is

---

[7] Available at https://github.com/trmrsh/trm-doppler
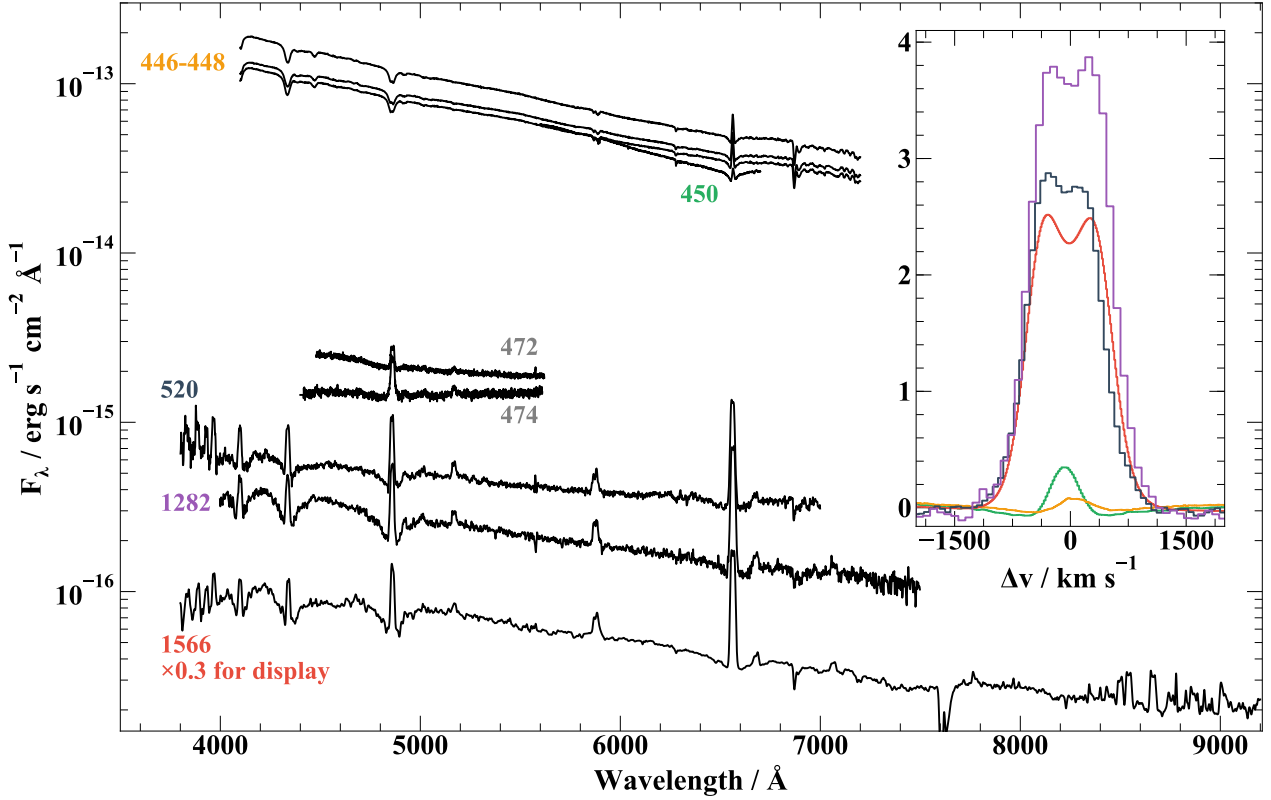
Figure 3. Optical spectral evolution throughout the superoutburst. We show the average spectrum for the corresponding epochs, labelled by our date notation, defined in Section 3. The GTC spectrum has been smoothed for clarity. *Inset:* The line profile evolution of Hα.
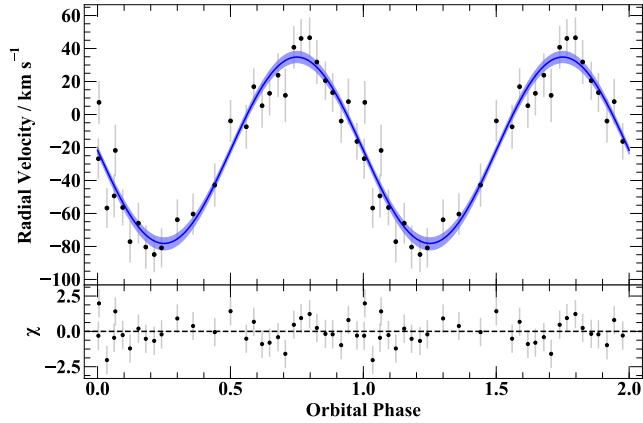

Figure 4. Radial Velocity curve of Hα in quiescence for the GTC spectra. Radial velocities were obtained via 2–Gaussian technique. The best fit is shown as the blue line and 1σ error bars have been scaled so $\chi^2_\nu = 1$.

shown in Fig. 6, where we show the broad absorption wings of the Balmer series. We used this relation and obtained $T_{eff} = 11,600 \pm 400$ K for the WD temperature and a power law index of $\Gamma = -1.40 \pm 0.1$. The accretion disc contributes $41\pm5\%$ of the optical light in this region, similar to other short orbital period systems (Aviles et al. 2010; Zharikov et

al. 2013). The contribution of the disc is lower at later epochs ($\sim 10\%$), when the system reaches its pre-outburst flux level, assuming the WD temperature does not cool down significantly during this period. However, the lack of spectroscopy at later date prevents us to confirm this scenario.

We can also approximate the observed quiescent accretion disc spectrum using a spectrum of the optically thin slab which mimics the radiation of the quiescent disc. We used simplified one-zone approximation for the spectrum calculation, considering homogeneous slab. The spectrum was computed using the well known solution for the homogeneous slab $F_\lambda = \pi B_\Lambda (1 - \exp(-\kappa_\lambda(T, \rho) * \rho * z))$, where z is the geometrical slab thickness, ρ is the matter density in the slab, and T is the slab temperature. The true opacity κ_λ was computed in LTE approximations using corresponding subroutines from Kurucz's code ATLAS (Kurucz 1970, 1993) adopted by V. Suleimanov (Suleymanov 1992; Ibragimov et al. 2003; Suleimanov & Werner 2007). The true opacity means that we considered only bound-bound, bound-free, and free-free transitions and ignored electron scattering. The slab parameters were tuned by hand to find the ones for which the model shows the best agreement with the observations. The accepted parameters are $T = 28\,4000$ K, $z = 5 \times 10^6$ cm, $\rho = 5.7 \times 10^{-10}$ g cm^{-3}, and $V \sin i = 518$ km s^{-1}. The derived size of the slab is $R_{\rm sl} \sqrt{\cos i} = 2.34 \times 10^9$ cm. We assumed that the slab has the solar chemical composition. We note that the calculated slab spectrum is in agreement
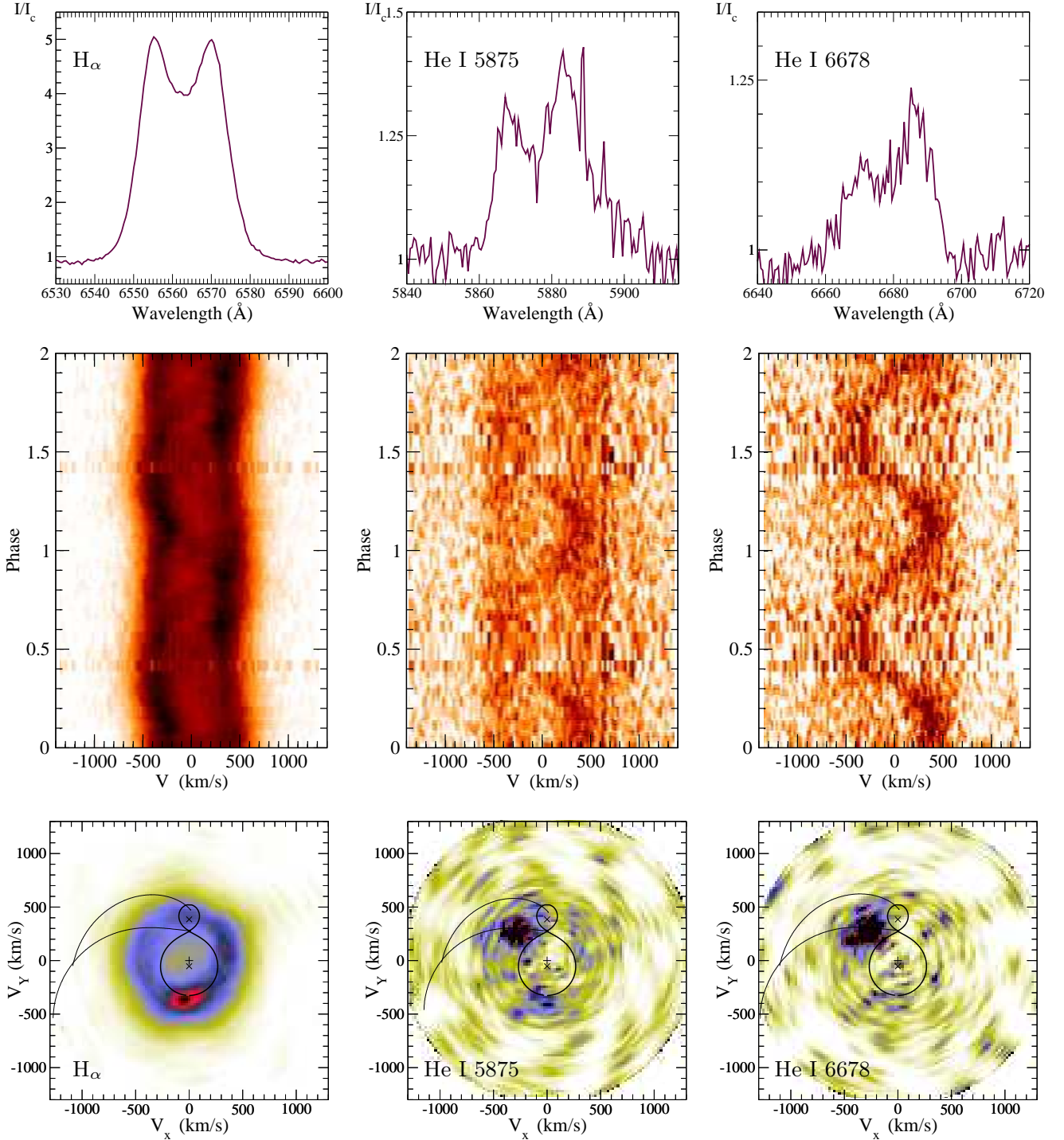
Figure 5. Time-resolved spectra of V1838 Aql during quiescence for Hα, He I 5875Å and 6678Å. For each line we show the median line profile (*top*), trail spectra (*middle*), and Doppler tomogram reconstructed for each line (*bottom*). The Roche lobe surface for the donor (solid line) and primary (dotted line) were calculated using following orbital parameters: $i = 60°$, $q = 0.1$ and $\gamma = -28$ km s^{-1}. The Keplerian and ballistic trajectories in the figure are marked as the upper and lower curves, respectively. The crosses are the velocity (from top to bottom) of the secondary star, the centre of mass and the primary star.
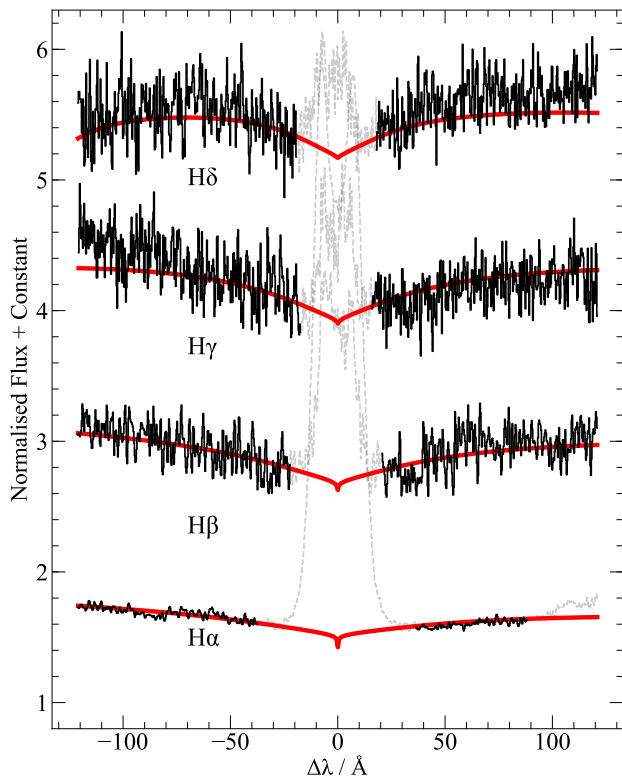
Figure 6. WD atmosphere model best fit (red) of the Balmer series wings. The emission core originating from the accretion disc has been masked. An arbitrary offset has been applied for clarity.

with the power law fit obtained above, but shows less contribution to the total system flux in the NIR wavelengths.

Initially, we independently calculated the distance to V1838 Aql previous to the *Gaia* DR2 release. Using the mean value of the absolute magnitude of 340 White Dwarfs in binary systems from the catalogue of McCook–Sion (McCook & Sion 1999), we obtained a mean equal to $\langle M \rangle = 12.61$. We assumed that the brightness of the accretion disc of a period bouncer system contributes from $\sim 20 - 40\%$ of the brightness of the primary star (Aviles et al. 2010; Zharikov et al. 2013). The faintest magnitude observed for V1838 Aql is ($V = 18.6$), combined with the mean absolute magnitude obtained from the McCook–Sion catalogue, we find a distance interval 187 ± 50 pc, consistent with the distance measured afterwards by *Gaia*.

The temperature of the WD is both consistent with theoretical predictions (Townsley & Bildsten 2003; Knigge et al. 2011) and observational estimates for systems close to the period minimum (Zharikov & Tovmassian 2015; Pala et al. 2017). Furthermore, the measured T_{eff} lies within the instability strip, where pulsations are observed in isolated (Gianninas et al. 2006) and accreting WDs (e.g. GW Lib, Szkody et al. 2010). Future high-time resolution photometry in the ultraviolet or blue optical bands might provide a new candidate to study non-radial pulsations in WDs (e.g. Uthas et al. 2012).

5 DISCUSSION

5.1 Approaching or receding the period minimum?

Both theoretical predictions and observations of the CV population show a sharp cut–off in the orbital period distribution at about 80 min, the so-called period minimum (Ritter & Kolb 1998; Gänsicke et al. 2009). V1838 Aql, with an orbital period about ~82 min (Kato et al. 2014a; Echevarría et al. 2019), is located within the spread of systems around the period minimum and therefore makes it difficult to establish if the system is approaching or leaving it (i.e. period bouncer).

The light curve of its first (and only) recorded superoutburst (with no normal outbursts detected) can help address this question. Its morphology (e.g. amplitude, duration), has similar features observed in other WZ Sge–type systems. We observe a sudden drop in flux (both in optical and X-rays, see Fig. 1), followed by a gradual decrease back to its quiescent level (likely from the steady cooling of the WD, e.g. Neustroev et al. 2017). In particular, we note the lack of rebrightenings in V1838 Aql which are present in most WZ Sge–type stars.

Following the empirical morphological classification of superoutburst light curves proposed by Imada et al. (2006), V1838 Aql belongs to the *type* D morphology (i.e. no rebrightenings and sudden flux drop). Kato (2015) ascribes this morphology classification to an evolutionary sequence from pre- to post- period minimum systems (C:D:A:B:E) and points out that *type* D might be closely associated with systems around the period minimum, but still in the upper branch of the $q - P_{orb}$ branch. This is consistent with the larger contribution in the NIR by the donor (see Section 5.2), which suggests V1838 Aql to be a pre-bounce system.

Another way to discern if a system is a period bouncer is to look for distinct features in quiescence such as permanent double-hump light curve as well as a spiral arm structure in their Doppler tomography (Zharikov & Tovmassian 2015). Echevarría et al. (2019) presented two light curves of V1838 Aql obtained in 2018 which do not show a double-hump modulation. However, the lack of a precise ephemeris prevents to further explore the presence of more subtle modulations. With regards to a spiral pattern, we observed a distinct feature in the accretion disc in a peculiar position of the velocity space (see Hα tomogram in Section 4.3). This feature however, is different to the ones observed in good period bouncer candidates as V406 Vir (Zharikov et al. 2008) or EZ Lyn (Zharikov et al. 2013), where a dual-emitting component was associated to spiral patterns in the disc. On the other hand, it resembles more to those found in HT Cas (e.g. Neustroev et al. 2016), as discussed further in Section 4.3. In any case, until the real phasing of the system is found no definitive conclusion on the origin of these structure can be drawn.

Period bouncers have small mass ratios ($q \lesssim 0.1$). In consequence, the more massive WD should present small semi-amplitudes, K_1, in their radial velocity curves. In order to test this for V1838 Aql it is necessary to estimate the inclination angle of the system. The quiescent spectrum clearly shows a double–peak emission on the Balmer series as well in the HeI which is observed in accretion discs with inclination angles $i \gtrsim 15°$ (Horne & Marsh 1986). Also, the lack of

eclipses in the photometry imposes an upper limit, for reasonable mass ratios of period bouncers, $i \lesssim 81°$ (for $q \simeq 0.05$, Bailey 1990). In addition, V1838 Aql shows small peak-to-peak separations ($\sim 650 - 700$ km s^{-1} for Hα) in contrast to eclipsing systems at similar orbital periods (e.g. ~ 1300 km s^{-1} for SDSS J1433+0038, Tulloch et al. 2009). Comparing this with other eclipsing short–periods CVs, we conclude that the inclination angle is relatively small ($i \sim 30°$) Thus, the *real* not projected semi-amplitude is very high ($K_1 \sim 100$ km s^{-1}). Assuming the q determination from superhumps (Echevarría et al. 2019), the donor in V1838 Aql would lie above the sub-stellar threshold. Again, this would argue for a pre-bounce system.

5.2 Low–mass star or sub–stellar donor?

The large wavelength range of the GTC spectrum allowed us to search for evidence of the donor (e.g. absorption features) as shown in Fig. 7. In particular, we searched in the region between 0.7–1 μm where the SED of the donor should start to contribute a significant percentage of the system's light. However, we find a wide range of the spectrum to be mostly dominated by broad emission Paschen lines. In the non–contaminated regions, we find no absorption features associated with the donor.

Despite the lack of evidence of features of the donor star in the optical region, the donor continuum should contribute as significant fraction at longer wavelengths. We used the multi-coloured broadband photometry in a true quiescent state to illustrate the type of donor expected from its NIR properties[8]. Theoretically, the orbital period suggests that the donor is likely to have a spectral type later than M6 ($T_2 \lesssim 2\,400$ K, Knigge 2006; Knigge et al. 2011) depending whether the system lies before or after the period minimum. We show in Fig. 7 two models using the fit done in the optical region (where the donor contribution is minimal) scaling down the power-law contribution to match the photometry and adding a low-mass star atmosphere model of 1 900 K and 2 200 K (Baraffe et al. 2015) appropriate for a pre- and post-period minimum system at P$_{orb} \sim 82$ min, respectively. No fit has been performed and only presented here as reference.

The photometry shows a flux increase starting at ~ 8000 Å, deviating from just the simple addition of a WD model and the power law. This excess in addition to the better match of the NIR fluxes to the hotter component suggests that V1838 Aql is indeed approaching the period minimum. However, a consistent fit with quasi-simultaneous data is needed to deliver a more accurate estimate of the properties of the donor. Thus, V1838 Aql is an ideal candidate for NIR time–resolved spectroscopy (e.g. Hernández Santisteban et al. 2016), which would render a fully independent measurement of the mass ratio and confirm or reject its sub–stellar

nature. This is particularly important since few systems have been characterised close to the period minimum, where the transition from stellar to sub-stellar regime is expected.

6 SUMMARY

We have presented a long–term photometric and spectroscopic study of the 2013 superoutburst of V1838 Aql from its peak to quiescence. The morphology of the outburst in combination with previous photometric estimates (Kato et al. 2014a; Echevarría et al. 2019) allow us to confirm V1838 Aql as a short orbital period system and provide updated ephemeris. A few days after the peak of the outburst, we discovered extended emission around the object, as observed in the high-resolution spectroscopy. Further deep Hα revealed an illuminated bow shock consistent with the proper motion of the object (123 ± 5 km s^{-1}). Although the origin of the material that creates the bow-shock is unclear, we conclude that a quasi-continuous outflow of material (~ 1000 km s^{-1}) is required to sustain a standing bow shock with the ISM.

In quiescence, we obtained time–resolved spectroscopy which allowed us to determine a semi–amplitude of the primary $K_1 = 53 \pm 3$ km s^{-1}. Doppler tomography in Hα revealed an emission component inconsistent with the ballistic trajectory of the accretion stream observed in the He I lines. Further observations and refinement of the ephemeris are needed to discern the origin of this emitting component. The broad band spectroscopy, allowed us to infer the effective temperature of the primary $T_{eff} = 11\,600 \pm 400$ K. This is consistent with theoretical expectations (Townsley & Bildsten 2003) as well as observational constrains on similar systems (Pala et al. 2017).

A discussion is made on the possible period-bouncer nature of the object. The broadband optical and NIR photometry suggests that V1838 Aql is approaching the period minimum limit and hosts a $> 2\,000$ K donor. However, we point out that simultaneous optical and infrared time-resolved spectroscopy (or photometry) needs to be performed, in order to measure the radial velocity curves of both components and to determine the spectral type of the donor star and its possible sub-stellar nature.

---

[8] We note that at the time of the GTC spectrum (day 1566), the system is slightly brighter than its pre-outburst state taken by PAN-STARRS1 in 2012 and a later observation taken with the NTT (day 2032). Unfortunately, we do not have information of the NIR flux close to the GTC epoch. This suggests that even 3 years after the superoutburst, either the WD is still cooling or the disc remains brighter.
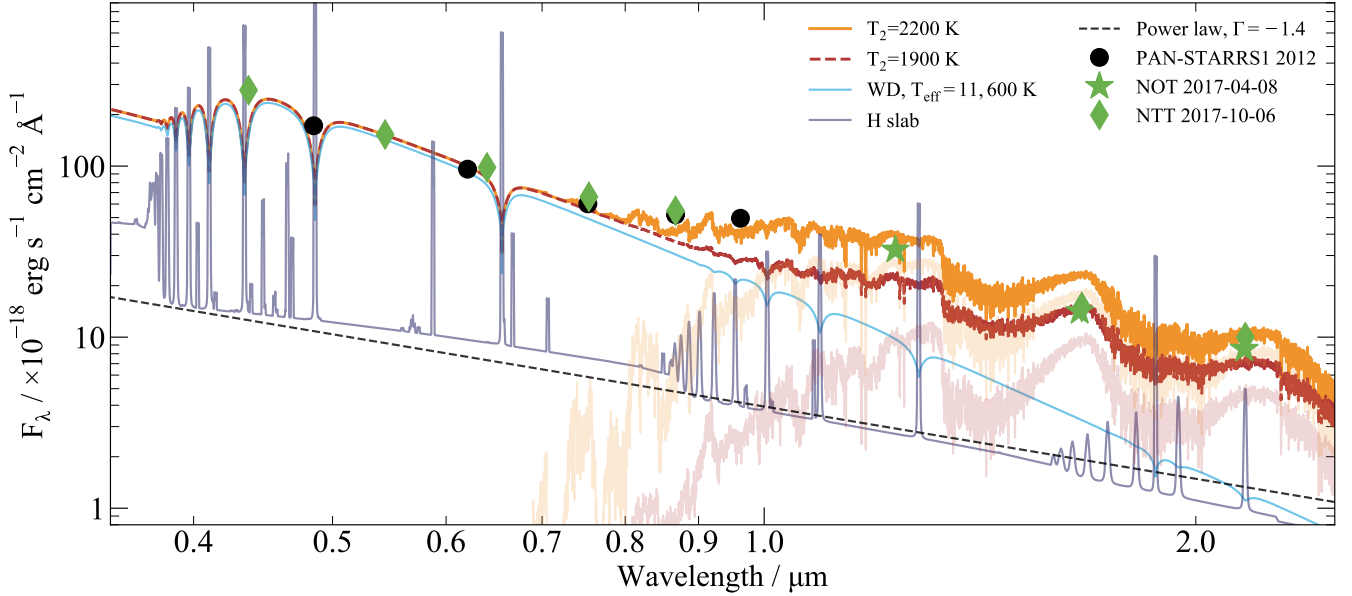
Figure 7. Broadband SED of V1838 Aql in quiescence. We show the multi-band photometry before (PAN-STARRS) and post-outburst (NOT and NTT). Two models have been scaled to compare the NIR contribution of the donor using low-mass star atmospheres of 2200 K (red) and 1900 K (orange), corresponding to a pre and post-bounce system (Knigge et al. 2011) respectively. The WD and power law index are taken from the Balmer wing fit. The power law contribution has been scaled by hand to match the quiescent level ($\sim 10\%$ contribution). The thin slab model is also scaled down and show as reference.

REFERENCES

Astropy Collaboration, Robitaille, T. P., Tollerud, E. J., et al. 2013, A&A, 558, A33
Aviles, A., Zharikov, S., Tovmassian, G., et al. 2010, ApJ, 711, 389
Bailer-Jones, C. A. L., Rybizki, J., Fouesneau, M., Mantelet, G., & Andrae, R. 2018, AJ, 156, 58
Bailey, J. 1990, MNRAS, 243, 57
Baraffe, I., Homeier, D., Allard, F., & Chabrier, G. 2015, A&A, 577, A42
Bond, H. E., & Miszalski, B. 2018, PASP, 130, 094201
Breedt, E., Gänsicke, B. T., Drake, A. J., et al. 2014, MNRAS, 443, 3174
Buzzoni B., et al., 1984, Msngr, 38, 9
Chevalier, R. A., Kirshner, R. P., & Raymond, J. C. 1980, ApJ, 235, 186
Clarke, J. T., & Bowyer, S. 1984, A&A, 140, 345
Coppejans, D. L., Körding, E. G., Knigge, C., et al. 2016, MNRAS, 456, 4441
de Miguel, E., Patterson, J., Cejudo, D., et al. 2016, MNRAS, 457, 1447
Echevarría, J., de la Fuente, E. & Costero, R. 2007, AJ, 197, 565
Echevarría, J., de Miguel, E., Hernández Santisteban, J. V., et al. 2019, Rev. Mex. Astron. Astrofis., 55, 1. (arXiv:1810.09864)
Foreman-Mackey, D. 2017, Astrophysics Source Code Library, ascl:1702.002
Gaia Collaboration, Brown, A. G. A., Vallenari, A., et al. 2018, A&A, 616, A1
Gänsicke, B. T., Dillon, M., Southworth, J., et al. 2009, MNRAS, 397, 2170

Gehrels, N., Chincarini, G., Giommi, P., et al. 2004, ApJ, 611, 1005

Gianninas, A., Bergeron, P., & Fontaine, G. 2006, AJ, 132, 831

Goliasch, J., & Nelson, L. 2015, ApJ, 809, 80

Greiner J., et al. 2001, A&A, 376, 1031

Harrison, T. E. 2016, ApJ, 816, 4

Hellier, C. 2001, in *Cataclysmic Variable Stars*, Springer, Praxis Publishing, Chichester, UK, p. 165

Hernández Santisteban, J. V., Knigge, C., Littlefair, S. P., et al. 2016, Nature, 533, 366

Hernández Santisteban, J. V., Echevarría, J., Michel, R., & Costero, R. 2017, MNRAS, 464, 104

Hollis, J. M., Oliversen, R. J., Wagner, R. M., & Feibelman, W. A. 1992, ApJ, 393, 217

Horne, K., Wade, R. A., & Szkody, P. 1986, MNRAS, 219, 791

Horne, K. and Marsh, T. R. 1986, MNRAS, 218, 761

Howell, S. B., Rappaport, S., & Politano, M. 1997, MNRAS, 287, 929

Howell, S. B., Hoard, D. W., Brinkworth, C., Kafka, S., Walentosky, M.J., Walter, F. M. & Rector, T.A. 2008, ApJ, 685, 418

Hubeny, I., & Lanz, T. 1995, ApJ, 439, 875

Hubeny, I., & Lanz, T. 2017, arXiv:1706.01859

Hunter, J. D. 2007, Computing In Science & Engineering, 9, 90

Hurst G. 2013, The Astronomer Electronic Circular, 2919

Ibragimov A. A., Suleimanov V. F., Vikhlinin A., Sakhibullin N. A., 2003, ARep, 47, 186

Imada, A., Kubota, K., Kato, T., Nogami, D., Maehara, H., Nakajima, K., Uemura, M., & Ishioka, R. 2006, PASJ, 58, 23

Itagaki, K. et al. 2013, CBET, 3554, 1

Kato T. 2015, PASJ, 67, 108

Kato, T., & Osaki, Y. 2013, PASJ, 65, 115

Kato T. et al. 2009, PASJ, 61, 395

Kato T. et al. 2014a, PASJ, 66, 90

Kato, T., et al. 2014b, PASJ, 66, 30

Klemola, A. R., Hanson, R. B., Jones, B. F., & Monet, D. G. 2004, VizieR Online Data Catalog, 1293,

Knigge, C. 2006, MNRAS, 373, 484

Knigge, C., Baraffe, I., & Patterson, J. 2011, ApJS, 194, 28

Kolb, U. & Baraffe, I. 1999, MNRAS, 309, 1034

Kurucz R. L., 1970, SAOSR, 309, 309

Kurucz R., 1993, KurCD, 13

Lang, D., Hogg, D. W., Mierle, K., Blanton, M., & Roweis, S. 2010, AJ, 139, 1782

Lenz P., & Breger M. 2005, Commun. Asteroseismol., 146, 53

Lindegren, L., Lammers, U., Bastian, U., et al. 2016, A&A, 595, A4

Littlefair, S. P., Dhillon, V. S., Marsh, T. R., et al. 2006, Science, 314, 1578

Marsh, T. R. 1988, MNRAS, 231, 1117

McCook, G. P. & Sion, E. M. 1999, ApJS, 121, 1

McLaughlin, D.B. 1960, in *Stallar Atmospheres*, ed. J.L. Greenstein, Univ. Chicago Press, Chicago, 585

Metzger, B. D., Hascoët, R., Vurm, I., et al. 2014, MNRAS, 442, 713

Moorwood A., Cuby J.-G., Lidman C., 1998, Msngr, 91, 9

Neustroev, V. V., & Zharikov, S. 2008, MNRAS, 386, 1366

Neustroev, V. V., Zharikov, S. V. & Borisov, N.V. 2016, A&A, 586, 10

Neustroev, V. V., Marsh, T. R., Zharikov, S. V., et al. 2017, MNRAS, 467, 597

Neustroev V. V., et al., 2018, A&A, 611, A13

Osaki, Y. 1974, PASJ, 26, 429

Osaki, Y. 1994, NATO Advanced Science Institutes (ASI) Series C, 417, 93

Osterbrock, D.E., Fulbright, J.P., Martel, A.R., Keane, M.J.& Trager S.C. 1996, PASP, 108, 277

Otulakowska–Hypka, M., Olech, A., & Patterson, J. 2016, MNRAS, 460, 2526

Paczynski, B., & Sienkiewicz, R. 1981, ApJ, 248, 27

Pala, A. F., Gänsicke, B. T., Townsley, D., et al. 2017, MNRAS, 466, 2855

Pala, A. F., Schmidtobreick, L., Tappert, C., Gänsicke, B. T., & Mehner, A. 2018, MNRAS,

Patterson, J. 1988, PASP, 110, 1132

Patterson, J. 2011, MNRAS, 411, 2695

Patterson, J. et al. 1996, PASP, 108, 748

Patterson, J. et al. 2005, PASP, 117, 1204

Patterson, J., Thorstensen, J. R., & Knigge, C. 2008, PASP, 120, 510

Paunzen, E., & Vanmunster, T. 2016, Astronomische Nachrichten, 337, 239

Reis R. C., Wheatley P. J., Gänsicke B. T., Osborne J. P., 2013, MNRAS, 430, 1994

Ritter, H. & Kolb, U. 1998, A&A, 128, 83

Robitaille, T., & Bressert, E. 2012, Astrophysics Source Code Library, ascl:1208.017

Sahman, D. I., Dihllon, V. S., Knigge, C. & Marsh, T. R. 2015, MNRAS, 451, 2863

Shafter, A. W., Szkody, P., & Thorstensen, J. R. 1986, ApJ, 308, 765

Skillman D.R., Patterson J. 1993, ApJ, 417, 298

Smak, J. 1993, Acta Astron., 43, 101

Stellingwerf, R. F. 1978, ApJ, 224, 953

Stetson, P. B. 1987, PASP, 99, 191

Suleymanov V. F., 1992, SvAL, 18, 104

Suleimanov V., Werner K., 2007, A&A, 466, 661

Szkody, P., Mukadam, A., Gänsicke, B. T., et al. 2010, ApJ, 710, 64

Tovmassian G., Gänsicke B., Zharikov S., Ramirez A., Diaz M. 2011, IAUS, 275, 311

Townsley, D. M., & Bildsten, L. 2003, ApJ, 596, 227

Tulloch, S. M., Rodríguez–Gil, P., & Dhillon, V. S. 2009, MNRAS, 397, 82

Uthas, H., Knigge, C., Long, K. S., Patterson, J., & Thorstensen, J. 2011, MNRAS, 414, 85

Uthas, H., Patterson, J., Kemp, J., et al. 2012, MNRAS, 420, 379

van Buren, D., & McCray, R. 1988, ApJ, 329, 93

Vogt, N. 1982, ApJ, 252, 653

Warner, B. 1995, *Cataclysmic Variable Stars*, (Cambridge University Press)

Weaver, R., McCray, R., Castor, J., Shapiro, P., & Moore, R. 1977, ApJ, 218, 377

Wilkin, F. P. 1996, ApJ, 459, 31

Yoon, D., & Heinz, S. 2017, MNRAS, 464, 3297

Zharikov, S., Tovmassian, G., Napiwotzki, R., Michel, R. \$ Neustroev, V. V. 2008, A&A, 449, 645

Zharikov, S., Tovmassian, G., Aviles, A., et al. 2013, A&A, 549, 77

Zharikov, S. & Tovmassian, G. 2015, Acta Polytechnica CTU Proceedings 2, 41

Zorotovic, M., Schreiber, M. R., & Gänsicke, B. T. 2011, A&A, 536, A42

APPENDIX A: *GAIA* POSTERIOR DISTRIBUTIONS

We present the joint and marginal posterior distributions of the *Gaia* distance and tangential velocity, shown in Fig. A1 (see Sec. 3.1). We used CORNER.PY (Foreman-Mackey 2017) to visualise the MCMC chains.
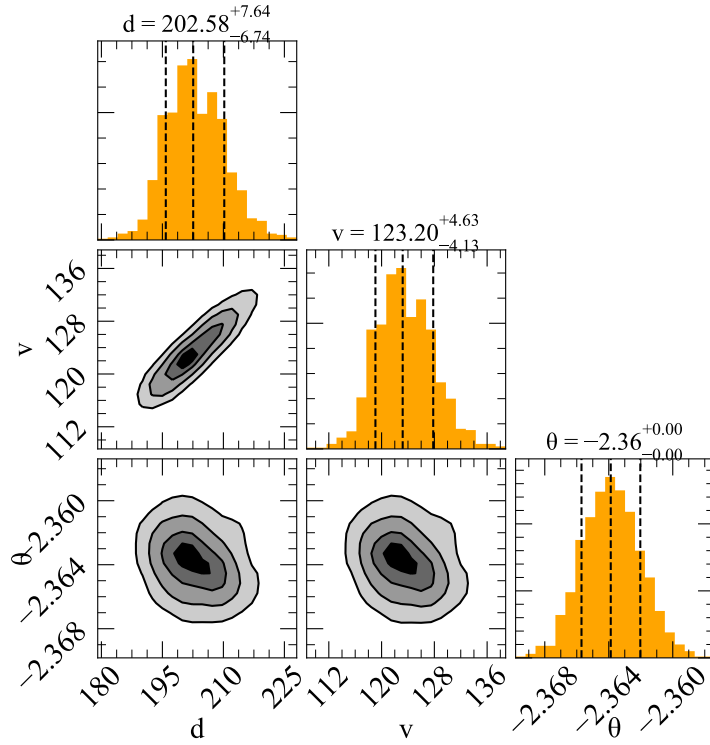
Figure A1. Posterior probability distributions for the *Gaia* distance and tangential velocity. Colour scale contours show the joint probability for every combination of parameters. Units for each parameter are: distance in pc, velocity in km s^{-1} and angle in radians. Contours represent the 0.5σ, 1σ , 2σ and 3σ levels. Marginal posterior distributions are shown as histograms with the median and 1σ marked as dashed lines.

This paper has been typeset from a T$_{\rm E}$X/LaT$_{\rm E}$X file prepared by the author.